

Inference-Time Text-to-Video Alignment with Diffusion Latent Beam Search

Yuta Oshima¹ Masahiro Suzuki¹ Yutaka Matsuo¹ Hiroki Furuta¹

Abstract

The remarkable progress in text-to-video diffusion models enables photorealistic generations, although the contents of the generated video often include unnatural movement or deformation, reverse playback, and motionless scenes. Recently, an alignment problem has attracted huge attention, where we steer the output of diffusion models based on some quantity on the goodness of the content. Because there is a large room for improvement of perceptual quality along the frame direction, we should address which metrics we should optimize and how we can optimize them in the video generation. In this paper, we propose *diffusion latent beam search with lookahead estimator*, which can select better diffusion latent to maximize a given alignment reward, at inference time. We then point out that the improvement of perceptual video quality considering the alignment to prompts requires *reward calibration* by weighting existing metrics. When evaluating outputs by using vision language models as a proxy of humans, many previous metrics to quantify the naturalness of video do not always correlate with evaluation and also depend on the degree of dynamic descriptions in evaluation prompts. We demonstrate that our method improves the perceptual quality based on the calibrated reward, without model parameter update, and outputs the best generation compared to greedy search and best-of-N sampling. We provide practical guidelines on which axes, among search budget, lookahead steps for reward estimate, and denoising steps, in the reverse diffusion process, we should allocate the inference-time computation.¹

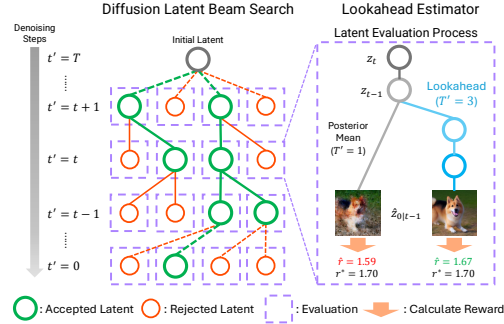


Figure 1. Diffusion latent beam search (DLBS) seeks a better diffusion path over the reverse process; sampling K latents per beam and possessing B beams for the next step, which mitigates the effect from inaccurate argmax. Lookahead estimator notably reduces the noise at latent reward evaluation by interpolating the rest of the time steps from the current latent with deterministic DDIM.

1. Introduction

The remarkable progress in text-to-video diffusion models enables photorealistic, high-resolution video generation (OpenAI, 2024; Google DeepMind, 2024; Chen et al., 2024; Blattmann et al., 2023a). Many future applications are anticipated such as creating novel games (Bruce et al., 2024), movies (Zhu et al., 2023), or simulators to control real-world robots (Brooks et al., 2024). However, the detailed contents of the generated video often include unnatural movement or deformation, reverse playback, and motionless scenes, which should not happen in the real world. For instance, simulating factual physics in the generated video is still challenging (Liu et al., 2024; Bansal et al., 2024). Recently, it has attracted a lot of attention to steering the output of diffusion models based on reward evaluation quantifying the goodness of the content, which is studied as an alignment problem (Lee et al., 2023b; Huang et al., 2024a). There is a large room for improvement of perceptual quality along the frame direction in the video, and to align models with our preference, we should address which metrics we should optimize and how we can optimize them.

In this paper, we propose *Diffusion Latent Beam Search* (DLBS) with *lookahead estimator*, an inference-time search over the reverse process (Figure 1), which can select better diffusion latent to maximize a given alignment reward. A lookahead estimator reduces the noise in reward estimate and a beam search robustly explores the latent paths avoid-

¹The University of Tokyo, Japan. Correspondence to: Yuta Oshima <yuta.oshima@weblab.t.u-tokyo.ac.jp>, Hiroki Furuta <furuta@weblab.t.u-tokyo.ac.jp>.

Preprint.

¹Website: <https://sites.google.com/view/t2v-dlbs>



Figure 2. Qualitative evaluation among different search methods. We test prompts from DEVIL-high (above) and DEVIL-static (below). DLBS-LA generates more dynamic, and prompt-aligned videos than GS or BoN.

ing inaccurate argmax operation.

We then point out that the improvement of perceptual video quality considering the alignment to prompts requires *reward calibration* of existing metrics (Huang et al., 2024b). When we evaluate outputs by leveraging capable vision language models (OpenAI, 2023; Gemini Team, 2023) as a proxy of human rater, many previous metrics to quantify the naturalness of video do not always correlate with each other, and optimal reward design to measure perceptual quality highly depends on the degree of dynamic descriptions in evaluation prompts. We design a weighted linear combination of multiple metrics, which is calibrated to perceptual quality and improves the correlation with preference.

We demonstrate that our method can induce high-quality outputs based on the calibrated reward or AI feedback (Figure 2), without model parameter update, and outputs the best generation under the same search budget compared to greedy search (Kim et al., 2024; Huang et al., 2024a) and best-of-N sampling (Zhang et al., 2024b; Ma et al., 2025). We also provide practical efficiency guidelines on which axes, among search budget, lookahead steps for reward estimate, and denoising steps, in the denoising process we should allocate the inference-time computation.

2. Preliminaries

Latent Diffusion Models Latent diffusion models (Rombach et al., 2022; Ma et al., 2024) are a special class of diffusion probabilistic models (Sohl-Dickstein et al., 2015; Ho et al., 2020), and popular choices for high-resolution text-to-video generation (He et al., 2022; Blattmann et al.,

2023b;a), which considers the diffusion process in embedding space. Let \mathbf{x}_0 as a video and encode it as $\mathbf{z}_0 = \text{Enc}(\mathbf{x}_0)$ using VAE (Kingma & Welling, 2013). Continuous-time forward diffusion process can be modeled as a solution to a stochastic differential equation (SDE) (Song et al., 2021b):

$$d\mathbf{z} = \mathbf{f}(\mathbf{z}, t)dt + g(t)d\mathbf{w}, \quad (1)$$

where $\mathbf{z}_0 \sim p_0(\mathbf{z})$ is the latent as initial condition while $p_t(\mathbf{z})$ is the marginal distribution of \mathbf{z}_t , $\mathbf{f} : \mathbb{R}^d \times \mathbb{R} \rightarrow \mathbb{R}^d$ is the drift coefficient, $g : \mathbb{R} \times \mathbb{R} \rightarrow \mathbb{R}$ is the diffusion coefficient, and $\mathbf{w} \in \mathbb{R}^d$ is d -dimensional standard Wiener process. $\mathbf{f}(\cdot, \cdot)$ and $g(\cdot)$ are designed appropriately for the marginal distribution to reach $p_T(\mathbf{z}) \approx \mathcal{N}(0, \mathbf{I})$ as $t \rightarrow T$ (Karras et al., 2022). Reverse diffusion process generates samples \mathbf{z}_0 through the following reverse-time SDE:

$$d\mathbf{z} = [\mathbf{f}(\mathbf{z}, t) - g(t)^2 \nabla_{\mathbf{z}} \log p_t(\mathbf{z})]dt + g(t)d\bar{\mathbf{w}}, \quad (2)$$

where dt here is an infinitesimal negative time step from T to 0 and $\bar{\mathbf{w}} \in \mathbb{R}^d$ is a standard reverse-time Wiener process. We start this with $\mathbf{z}_T \sim \mathcal{N}(0, \mathbf{I})$. This SDE induces the marginal distribution on the data $p^{\text{pre}}(\mathbf{z})$ (i.e. pre-trained diffusion models). While we omit the notation for simplicity, we consider the text-to-video generation problem, where the diffusion process is conditioned on text prompts \mathbf{c} .

Alignment for Text-to-Video Diffusion Models In this paper, we define the alignment problem in text-to-video generation as increasing the probability of generating perceptually good video for humans, such as $\max \mathbb{E}[p(\mathcal{O} = 1 | \mathbf{x}_0, \mathbf{c})]$ where $\mathcal{O} \in \{0, 1\}$ represents if the generated video \mathbf{x}_0 conditioned on \mathbf{c} is perceptually higher quality or not. The common assumption is such a probability depends on a proxy

scalar reward function $r(\mathbf{x}_0, \mathbf{c})$ such as $p(\mathcal{O} = 1 | \mathbf{x}_0, \mathbf{c}) \propto \exp(\beta^{-1} r(\mathbf{x}_0, \mathbf{c}))$ with $\beta \in \mathbb{R}$, and then the problem comes down to reward maximization. The proxy reward function may take generated video \mathbf{x}_0 and a prompt \mathbf{c} as inputs.

Alignment as Stochastic Optimal Control Previous works formulate such a reward maximization problem from the view of stochastic optimal control (Uehara et al., 2024; Huang et al., 2024a; Domingo-Enrich et al., 2024), where we aim to find an additional drift term $\mathbf{u}(\cdot, \cdot)$ for the following reverse SDE:

$$d\mathbf{z} = [\mathbf{f}(\mathbf{z}, t) - g(t)^2 \nabla_{\mathbf{z}} \log p_t(\mathbf{z}) + \mathbf{u}(\mathbf{z}, t)] dt + g(t) d\bar{\mathbf{w}}. \quad (3)$$

For convenience, we adopt the change-of-variables as $\boldsymbol{\nu}_t := \mathbf{z}_{T-t}$ and $\bar{\mathbf{f}}(\boldsymbol{\nu}, t) := \mathbf{f}(\boldsymbol{\nu}, t) - g(t)^2 \nabla_{\boldsymbol{\nu}} \log p_t(\boldsymbol{\nu})$ because stochastic control is often based on the standard flow of time ($t: 0 \rightarrow T$), and then Equation 3 is written as:

$$d\boldsymbol{\nu} = [\bar{\mathbf{f}}(\boldsymbol{\nu}, t) + \mathbf{u}(\boldsymbol{\nu}, t)] dt + g(t) d\mathbf{w}, \quad (4)$$

where dt here is an infinitesimal time step and $d\mathbf{w}$ is a standard Wiener process.

Because the alignment problem comes down to reward maximization, the objective in stochastic control literature is

$$\mathbf{u}^* = \underset{\mathbf{u}}{\operatorname{argmax}} \mathbb{E} \left[r'(\boldsymbol{\nu}_T) - \frac{\lambda}{2} \int_{t=0}^T \frac{\|\mathbf{u}(\boldsymbol{\nu}_t, t)\|^2}{g(t)^2} dt \right] \quad (5)$$

where $r'(\cdot) := r(\operatorname{Dec}(\cdot))$ evaluates the latent in the video space and $\lambda > 0$. The expectation is taken over samples from Equation 4. In stochastic control, it is known that we can define the optimal value function,

$$v_t^*(\boldsymbol{\nu}) = \mathbb{E}_{p^*} \left[r'(\boldsymbol{\nu}_T) - \frac{\lambda}{2} \int_{s=t}^T \frac{\|\mathbf{u}(\boldsymbol{\nu}_s, s)\|^2}{g(s)^2} ds \mid \boldsymbol{\nu}_t = \boldsymbol{\nu} \right], \quad (6)$$

where $p_t^*(\boldsymbol{\nu}) = \frac{1}{Z} \exp(\frac{v_t^*(\boldsymbol{\nu})}{\lambda}) p_t^{\text{pre}}(\boldsymbol{\nu})$, and obtain the optimal drift $\mathbf{u}^*(\boldsymbol{\nu}, t) = g(t)^2 \nabla_{\boldsymbol{\nu}} \frac{v_t^*(\boldsymbol{\nu})}{\lambda}$ (Pavon, 1989). This optimal value function is the solution of stochastic Hamilton-Jacobi-Bellman equation (Evans, 2022) according to this Feynman-Kac formula (Øksendal, 2003; Moral, 2004):

$$\exp\left(\frac{v_t^*(\boldsymbol{\nu})}{\lambda}\right) = \mathbb{E}_{p^{\text{pre}}} \left[\exp\left(\frac{r'(\boldsymbol{\nu}_T)}{\lambda}\right) \mid \boldsymbol{\nu}_t = \boldsymbol{\nu} \right] \quad (7)$$

and then we obtain a tractable form of optimal drift term as:

$$\mathbf{u}^*(\boldsymbol{\nu}_t, t) = g(t)^2 \nabla_{\boldsymbol{\nu}} \log \mathbb{E}_{p^{\text{pre}}} \left[\exp\left(\frac{r'(\boldsymbol{\nu}_T)}{\lambda}\right) \mid \boldsymbol{\nu}_t = \boldsymbol{\nu} \right]. \quad (8)$$

The intuition here is the optimal drift pulls the current latent $\boldsymbol{\nu}$, while following the pre-trained reverse SDE, into the region achieving a higher reward at time T .

Algorithm 1 Diffusion Latent Beam Search (DLBS) with Stochastic DDIM

Input: latent diffusion model ϵ_θ , reward function r' , noise scheduling parameter $\{\alpha_t\}_{t=0}^T, \{\sigma_t\}_{t=0}^T$, number of beams B , number of candidates K

- 1: $\mathbf{z}_T^1, \dots, \mathbf{z}_T^B \sim \mathcal{N}(\mathbf{0}, \mathbf{I})$ \triangleright Initial B beams
- 2: **for** $t = T$ **to** 1 **do**
- 3: **for** $j = 1$ **to** B **do**
- 4: \triangleright Compute the posterior mean of \mathbf{z}_{t-1}^j
- 5: $\hat{\mathbf{z}}_{0|t}^j = \frac{1}{\sqrt{\alpha_t}} (\mathbf{z}_t^j - \sqrt{1 - \alpha_t} \epsilon_\theta(\mathbf{z}_t^j))$
- 6: $\mathbf{z}_{t-1}^j = \sqrt{\alpha_{t-1}} \hat{\mathbf{z}}_{0|t}^j + \sqrt{1 - \alpha_{t-1} - \sigma_t^2} \epsilon_\theta(\mathbf{z}_t^j)$
- 7: **end for**
- 8: **if** $t > 1$ **then**
- 9: **for** $j = 1$ **to** B **do**
- 10: \triangleright Sample K next candidate latents
- 11: $\mathbf{z}_{t-1}^{ij} = \mathbf{z}_{t-1}^j + \sigma_t \epsilon_t^i$ with $\epsilon_t^1, \dots, \epsilon_t^K \sim \mathcal{N}(\mathbf{0}, \mathbf{I})$
- 12: \triangleright Estimate the clean sample from noisy latent
- 13: $\hat{\mathbf{z}}_{0|t-1}^{ij} = \frac{1}{\sqrt{\alpha_{t-1}}} (\mathbf{z}_{t-1}^{ij} - \sqrt{1 - \alpha_{t-1}} \epsilon_\theta(\mathbf{z}_{t-1}^{ij}))$
- 14: **end for**
- 15: \triangleright Search B higher-reward beams from KB latents
- 16: budget := $\{(\mathbf{z}_{t-1}^{11}, \hat{\mathbf{z}}_{0|t-1}^{11}), \dots, (\mathbf{z}_{t-1}^{KB}, \hat{\mathbf{z}}_{0|t-1}^{KB})\}$
- 17: **for** $j' = 1$ **to** B **do**
- 18: $\mathbf{z}_{t-1}^{j'} = \operatorname{argmax}_{\mathbf{z}_{t-1}^{ij} \in \text{budget}} r'(\hat{\mathbf{z}}_{0|t-1}^{ij})$
- 19: budget = budget $\setminus \{(\mathbf{z}_{t-1}^{j'}, \hat{\mathbf{z}}_{0|t-1}^{\operatorname{argmax}})\}$
- 20: **end for**
- 21: $j \in \{1, \dots, B\} \leftarrow j' \triangleright$ Reset selected B indices
- 22: **end if**
- 23: **end for**
- 24: **return:** $\mathbf{z}_0 = \operatorname{argmax}_{\mathbf{z}_0^j \in \{\mathbf{z}_0^1, \dots, \mathbf{z}_0^B\}} r'(\mathbf{z}_0^j)$

3. Diffusion Latent Beam Search

We first provide a unified view of existing inference-time alignment methods through several practical approximations of optimal drift $\mathbf{u}^*(\boldsymbol{\nu}_t, t)$ (Section 3.1). To mitigate errors from those approximations, we propose a novel inference-time search algorithm, *diffusion latent beam search* with *lookahead estimator* (Section 3.2).

3.1. A Unified View for Practical Approximations

While Equation 8 has a relatively tractable form, it is still computationally expensive, since the expectation requires full diffusion sampling to evaluate latent at each time step, as well as facing numerical instability. Previous alignment methods rely on multiple-step practical approximations.

Step 1: Jensen’s Inequality First, when assuming $\frac{r'(\boldsymbol{\nu}_T)}{\lambda}$ is almost deterministic (this might hold when $t \rightarrow T$), Jensen’s inequality yields the following approximation by

Algorithm 2 Lookahead (LA) with Deterministic DDIM

Input: latent diffusion model ϵ_θ , current diffusion latent \mathbf{z}_{t-1} , number of lookahead steps $T' (\ll T)$

- 1: \triangleright Run T' -step deterministic DDIM starting from \mathbf{z}_{t-1}
- 2: $\tilde{t}(s) \in \{t-1, \dots, \lfloor \frac{s}{T'}(t-1) \rfloor, \dots, \lfloor \frac{1}{T'}(t-1) \rfloor, 0\}$
- 3: Select new lookahead noise schedule $\{\tilde{\alpha}_s\}_{s=0}^{T'}$ for T' -step interpolation of the rest of original $\{\alpha_{t'}\}_{t'=0}^{t-1}$
- 4: $\mathbf{z}_{\tilde{t}(T')} := \mathbf{z}_{t-1}$
- 5: $\tilde{\mathbf{z}}_{0|\tilde{t}(T')} = \frac{\mathbf{z}_{\tilde{t}(T')} - \sqrt{1 - \tilde{\alpha}_{T'}} \epsilon_\theta(\mathbf{z}_{\tilde{t}(T')})}{\sqrt{\tilde{\alpha}_{T'}}$
- 6: **for** $s = T'$ **to** 1 **do**
- 7: $\mathbf{z}_{\tilde{t}(s-1)} = \sqrt{\tilde{\alpha}_{s-1}} \tilde{\mathbf{z}}_{0|\tilde{t}(s)} + \sqrt{1 - \tilde{\alpha}_{s-1}} \epsilon_\theta(\mathbf{z}_{\tilde{t}(s)})$
- 8: $\tilde{\mathbf{z}}_{0|\tilde{t}(s-1)} = \frac{\mathbf{z}_{\tilde{t}(s-1)} - \sqrt{1 - \tilde{\alpha}_{s-1}} \epsilon_\theta(\mathbf{z}_{\tilde{t}(s-1)})}{\sqrt{\tilde{\alpha}_{s-1}}}$
- 9: **end for**
- 10: **return:** $(\mathbf{z}_{t-1}, \tilde{\mathbf{z}}_{0|\tilde{t}(0)}) \triangleright$ Latent and LA estimator

exchanging log and $\mathbb{E}[\cdot]$, which can be considered as a certain form of classifier guidance (Dhariwal & Nichol, 2021):

$$\mathbf{u}^*(\boldsymbol{\nu}_t, t) \approx \frac{g(t)^2}{\lambda} \nabla_{\boldsymbol{\nu}} \mathbb{E}_{p^{\text{pre}}} [r'(\boldsymbol{\nu}_T) | \boldsymbol{\nu}_t = \boldsymbol{\nu}]. \quad (9)$$

Step. 2: Tweedie’s Formula To avoid the computationally expensive expectation, the expected reward is further approximated as $\mathbb{E}_{p^{\text{pre}}} [r'(\boldsymbol{\nu}_T) | \boldsymbol{\nu}_t = \boldsymbol{\nu}] \approx r'(\hat{\boldsymbol{\nu}}_{T|t})$ where $\hat{\boldsymbol{\nu}}_{T|t} \approx \mathbb{E}_{p^{\text{pre}}} [\boldsymbol{\nu}_T | \boldsymbol{\nu}_t = \boldsymbol{\nu}]$ is a one-step approximation of posterior mean (Chung et al., 2023), which can be calculated only with the current latent $\boldsymbol{\nu}_t$ without full diffusion path. Therefore, the optimal drift term can be seen as solely depending on the current time step t :

$$\mathbf{u}^*(\boldsymbol{\nu}_t, t) \approx \frac{g(t)^2}{\lambda} \nabla_{\boldsymbol{\nu}} r'(\hat{\boldsymbol{\nu}}_{T|t}). \quad (10)$$

Such a computationally tractable drift term has been leveraged for previous inference-time alignment methods via approximate guidance or twisted sequential Monte Carlo (SMC) (Wu et al., 2024b). However, as the approximated posterior mean $\hat{\boldsymbol{\nu}}_{T|t}$ in intermediate steps is noisy, evaluation with the reward function for clean data $r'(\cdot)$ may not provide a reliable signal (Liang et al., 2024). Moreover, Equation 10 requires the reward gradient, which is not applicable to non-differentiable reward, such as AI feedback, and is also not suitable for the modality whose reward gradient imposes a huge computational cost in practice, such as video.

Step. 3: Converting Reward Gradient into argmax The usage of reward gradient can be converted into argmax operator (Huang et al., 2024a; Li et al., 2024b; Bansal et al., 2023). The intuition here is since the optimal drift in Equation 10 induces the diffusion latent to the direction where it maximizes the reward, we replace such a maximization

with a zeroth-order search. The SDE is approximated as:

$$d\boldsymbol{\nu} = \bar{\mathbf{f}}(\boldsymbol{\nu}, t) dt + g(t) d\mathbf{w}^* \quad \text{where } d\mathbf{w}^* = \underset{d\mathbf{w}}{\operatorname{argmax}} r'(\hat{\boldsymbol{\nu}}_{T|t}). \quad (11)$$

Note that the current diffusion latents $\boldsymbol{\nu}_t$ and posterior mean $\hat{\boldsymbol{\nu}}_{T|t}$ are sampled by following the standard Wiener process $d\mathbf{w}$. This approximation is leveraged for inference-time alignment via greedy search (Huang et al., 2024a; Li et al., 2024b) or SMC (Singhal et al., 2025) of diffusion latents. However, greedy search can result in sub-optimal generation affected by inaccurate reward estimate $r'(\hat{\boldsymbol{\nu}}_{T|t})$ due to its noisy input. Moreover, for the high-dimensional domain, such as video generation, it can be challenging to get an accurate density ratio term required in SMC.

3.2. Mitigating Approximation Errors via Beam Search

Existing practical algorithms based on these three approximations, such as greedy search (Huang et al., 2024a; Li et al., 2024b), fall into sub-optimal generation due to the erroneous reward evaluation with a noisy estimate of the posterior mean (Chung et al., 2023), and argmax operator based on them. To resolve the error accumulation, we propose a simple yet robust modification, *diffusion latent beam search (DLBS)* with *lookahead estimator*. To clearly describe the practical implementation, we use the notation of discrete-time diffusion process in the rest of the section.

Practical Implementation We summarize the detailed sampling procedure of DLBS in Algorithm 1. For the diffusion sampler, we use stochastic DDIM (Song et al., 2021a) with a decreasing sequence $\{\alpha_t\}_{t=1}^T \in (0, 1]^T$, noise level η , and noise schedule $\sigma_t = \eta \sqrt{(1 - \alpha_{t-1}) / (1 - \alpha_t)} \sqrt{1 - \alpha_{t-1} / \alpha_t}$, which is equivalent to DDPM (Ho et al., 2020) when $\eta = 1.0$. We initialize B latent beams from the Gaussian distribution (Line 1.1), sample K latents per beam in next time step (Line 1.11), and then compute the one-step estimation of the posterior mean (Line 1.13). DLBS evaluates the estimator of posterior mean $\hat{\mathbf{z}}_{0|t-1}$ with reward function (Line 1.18) and selects Top- B -rewarded latent beams instead of Top-1 (i.e., argmax) from KB candidates (Line 1.19), which is iterated over entire reverse process from $t = T$ to $t = 0$. DLBS can possess latent beams more widely than greedy search under the same budget, which mitigates error propagation due to the approximated diffusion latent evaluation.

Lookahead Estimator The other source of approximation errors than argmax operator is a one-step estimator of the posterior mean $\hat{\mathbf{z}}_{0|t-1}$ from Tweedie’s formula, which is still noisy, especially in earlier time steps and leads to inaccurate reward evaluation. To reduce errors in reward evaluation, we propose a lookahead (LA) estimator $\tilde{\mathbf{z}}_{0|\tilde{t}(0)}$, which is estimated by running T' -step deterministic DDIM ($1 < T' \ll T$) while equally interpolating the rest of time steps

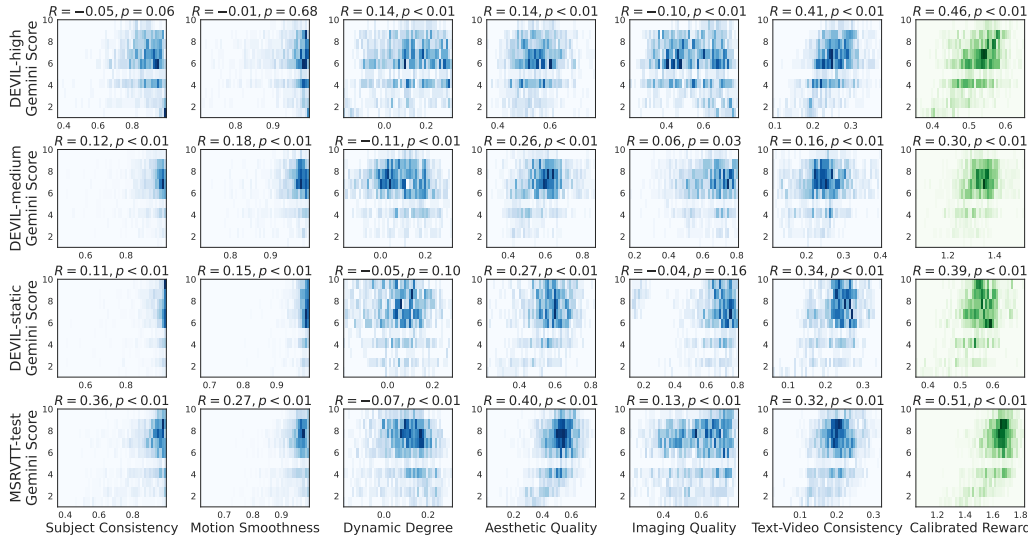


Figure 3. 2D-histogram and correlation between reward functions for perceptual video quality (Huang et al., 2024b) and AI feedback from Gemini (Gemini Team, 2023). A single reward (e.g., subject consistency; blue) is often not aligned well with a preference from Gemini, which happens for all the prompt sets with different degree of dynamics. The calibrated reward, a linear combination of perceptual metrics via brute-force search (green), achieves the best Pearson correlation coefficient in all settings (statistically significant with $p < 0.01$).

from the current latent \mathbf{z}_{t-1} to \mathbf{z}_0 (Algorithm 2). While requiring additional denoising steps, its cost is almost the same as naive DLBS because most computational costs come from when we decode \mathbf{z}_0 (i.e. reward evaluation). This more “accurate” estimator significantly improves the performance even with $T' = 2$ or 3 (Section 5.2).

4. Calibrating Reward to Preference Feedback

One of the most useful assessments for generative models is human evaluation, yet gathering human feedback at scale is prohibitively costly. A practical approach to reduce the time and cost is to leverage AI feedback from VLMs (Wu et al., 2024d), which has been shown to align with human judgment on video quality to some extent (Na et al., 2024; Furuta et al., 2024b). In this work, we assume that the VLM evaluation works as an oracle and we align model outputs to the preference of VLMs, which is reasonable due to their capability and the cost to be saved. Our qualitative evaluation also confirms that the high-rating video by VLMs is good for us. It is possible to replace VLMs with humans in our framework if the cost allows.

However, because alignment via inference-time search requires massive reward evaluation queries, we still need to build more tractable proxy rewards not relying on humans or external VLM APIs. The question here is what kind of metrics for perceptual video quality can improve the feedback from VLMs. Because the criteria of videos preferable to humans are multi-objective, maximizing a single metric may lead to undesirable generation due to over-optimization. In this section, we first review the possible video quality metrics (Section 4.1), evaluate the Pearson correlation be-

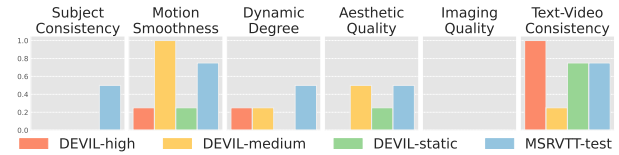


Figure 4. The coefficient of calibrated reward w_i with feedback from Gemini. Each set of prompts depicting different degree of dynamics requires different mixture of perceptual video qualities.

tween these and VLM feedback score, and then propose a reward calibration (Section 4.2), aiming to align the existing video rewards to VLMs by considering their weighted linear combination through the brute-force search of coefficients.

4.1. Metric Reward for Perceptual Video Quality

Following Huang et al. (2024b), we select six base reward functions for perceptual video quality (see Appendix B):

Subject Consistency quantifies how consistently the subject appears across video frames with DINO (Caron et al., 2021).

Motion Smoothness leverages the motion prior in AMT (Li et al., 2023) to evaluate whether the generated video’s motion is smooth and physically plausible.

Dynamic Degree quantifies the overall magnitude of dynamic object movement by estimating optical flow (Teed & Deng, 2020) for each pair of consecutive frames.

Aesthetic Quality measures compositional rules, color harmony, and the overall artistic merit of each video frame with LAION aesthetic predictor (LAION-AI, 2022).

Imaging Quality assesses low-level distortions (e.g., over-exposure, noise, blur) in each frame with MUSIQ predic-

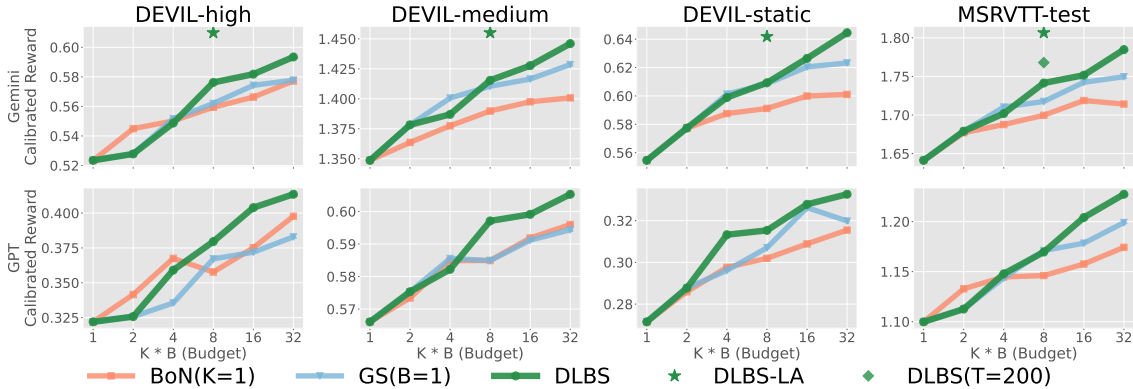


Figure 5. Comparison among diffusion latent beam search (DLBS), best-of-N (BoN) and greedy search (GS). We measure the performance in terms of a combinational reward calibrated to Gemini (above) and GPT-4o (below). DLBS improves all the calibrated reward the best as the search budget KB increases (especially $KB = 16, 32$) while BoN and GS in some cases eventually slows down or saturates the performance. Notably, LA estimator ($KB = 8, T' = 6$) is comparable to or even outperforming DLBS ($KB = 32$).

tor (Ke et al., 2021).

Text-Video Consistency captures how closely a content in a video aligns with a prompt with ViCLIP (Xu et al., 2021).

Reward Calibration To reflect the multi-dimensional aspect of preferable videos, we model the calibrated reward function $r^*(\cdot, \cdot)$ as a weighted linear combination of video quality metrics: $r^*(\mathbf{x}_0, \mathbf{c}) := \sum_{i=1}^M w_i r_i(\mathbf{x}_0, \mathbf{c})$. The coefficient w_i is determined by maximizing the Pearson correlation with preference feedback. We heuristically conduct a brute-force search within a reasonable range (Section 4.2).

Experimental Setup We leverage GPT-4o (OpenAI, 2023) and Gemini-1.5 (Gemini Team, 2023) as automated raters for generated videos. We provide a text prompt and generated video as inputs, instructing VLMs to assign discrete scores (1–10) based on overall visual quality (including clarity, resolution, brightness, and aesthetic appeal), the appropriateness of motion for either static or dynamic scenes, the smoothness and consistency of shapes and motions, and the degree of alignment with a prompt (see Appendix E).

We select four prompt sets from two distinct dataset (see Appendix C). DEVIL (Liao et al., 2024) classifies its prompts into five categories depending on the degree of movement, each further divided by subject type (e.g., cat, horse, truck, nature, etc.). We focus on three of five categories (static, medium, and high) and select one prompt at random from each subject-subdivision within a chosen category. We also draw 30 random captions from the test split of MSRVTT (Xu et al., 2016), widely used as a video benchmark.

To examine the correlation among AI feedback and perceptual quality metrics, we generate 64 videos per prompt from pre-trained Latte (Ma et al., 2024) using DDIM sampler with $T = 50$ and $\eta = 0.0$. We also prepare candidates of the calibrated reward by choosing the combination of weights $w_i \in \{0.0, 0.25, 0.5, 0.75, 1.0\}$ and use those later

to rank them based on the correlation with AI feedback.

4.2. Correlation and Reward Calibration

Figure 3 illustrates the 2D-histogram and corresponding correlation between each individual metric and feedback from Gemini (see Appendix F for GPT-4o). Relying on a single metric often yields low correlation, which supports the multifaceted nature of perceptual video quality. In addition, the relative importance of each metric depends on the movement in the prompts; in highly-dynamic DEVIL-high, dynamic degree correlates more strongly with VLMs than consistency metrics. Conversely, in less-dynamic DEVIL-medium or DEVIL-static, subject consistency and motion smoothness play more prominent roles. Because the aesthetic score focuses on frame-by-frame visual quality, it tends to exhibit a stronger correlation with VLM in low-motion scenarios, while rapid movements and frequent transitions often introduce motion blur or abrupt changes in composition, reducing the frame-level aesthetic quality and thus weakening its correlation with VLMs.

Notably, a weighted linear combination of these metrics yields the highest correlation with Gemini (Figure 3, green). Among brute-force candidates, we select the best coefficients in terms of correlation with Gemini per a set of prompts in Figure 4, which differ based on the degree of movement in the prompts. The dynamic degree and motion smoothness exhibit pronounced variation among DEVIL-high, -medium, and -static, and the weights of other factors, such as text-video consistency, subject consistency, and aesthetic considerations, are also adjusted to the prompts accordingly. This underscores the importance of appropriately weighting multiple evaluation criteria through the reward calibration.

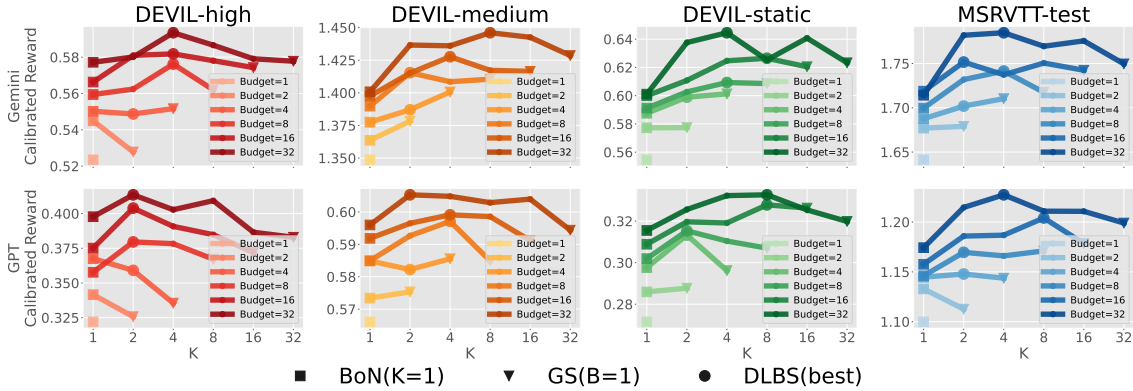


Figure 6. DLBS can improve the performance in any prompts or reward, as we increase the search budget $KB \in \{1, 2, 4, 8, 16, 32\}$. In addition, we can see an optimal balance between the number of latent K and the number of beam B under the same budget. For instance, as we increase the budget to $KB = 16$, we have a peak around $K = 4$ or $K = 8$, which is about 25–50% of the budget.

5. Inference-Time Text-to-Video Alignment

Experimental Setup We compare following inference-time search methods with a noise level $\eta = 1.0$ for DDIM:

- **Best-of-N Sampling (BoN):** We initialize B latents and they follow the reverse process independently ($K = 1$). At $t = 0$, we evaluate the reward and select the best.
- **Greedy Search (GS):** At each denoising step, we select the best-rewarded diffusion latent ($B = 1$) from K candidates sampled in a reverse process.
- **DLBS:** Given the budget KB , we sweep possible combinations in terms of multiple of 2 (e.g., $K = 4, B = 4$ or $K = 8, B = 2$), and then report the best results except for the case with $K = 1$ and $B = 1$.
- **DLBS-LA:** We combine DLBS with lookahead estimator from 6-step deterministic DDIM. Due to the resources, we have experiments with $KB = 8$.

We use the same prompt sets as in Section 4, and Gemini/GPT-calibrated rewards in Section 4.2. Note that the range of values may be different from each other as they have different coefficients. We test the performance when scaling (1) search budget KB (Section 5.1), (2) LA steps T' for reward estimate (Section 5.2), and (3) denoising steps (Section 5.3). We further analyze whether DLBS maximizing reward calibrated to VLMs can actually improve VLM evaluation (Section 5.4), and how the diversity of generated samples is in the inference-time search (Section 5.5).

5.1. Scaling Search Budget

Figure 5 measures the combinational reward calibrated to Gemini (above) and GPT-4o (below) while increasing the search budget $KB \in \{1, 2, 4, 8, 16, 32\}$. DLBS improves all the calibrated rewards the best as KB increases (especially $KB = 16, 32$) while BoN and GS in some cases eventually slow down or saturate the performance. See Appendix H for the results with $KB = 64$ in DEVIL-medium

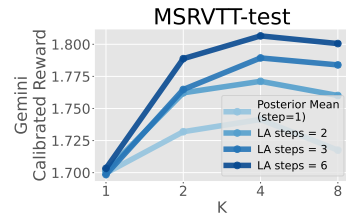


Figure 7. Comparison among different LA steps T' on MSRVTT-test ($KB = 8$). The performance improves, as increasing LA steps. Even $T' = 2$ significantly outperforms the posterior mean.

where we still observe the improvement.

Figure 6 demonstrates the scaling trend of DLBS, proportional to the search budget, under various choices of K . The results show that there is an optimal balance between the number of latent K and the number of beam B under the same budget. For instance, as we increase the budget to $KB = 16, 32$, we have a peak around $K = 4, 8, 16$, which is about 25–50% of the budget. This implies that balancing possession and exploration of diffusion latents in DLBS help search for the best outputs robustly.

5.2. Scaling Lookahead Steps for Reward Estimate

We scale up LA steps T' to obtain an accurate reward estimate. We use MSRVTT-test ($KB = 8$) and Gemini reward for experiments. Figure 7 shows that as increasing LA steps, the performance improves more. Even $T' = 2, 3$ significantly outperforms the posterior mean, which is often used in prior works (Kim et al., 2024; Huang et al., 2024a; Singhal et al., 2025). This is because the sub-optimal performance of inference-time search comes from the approximation errors and LA estimator can notably reduce them. Moreover, as shown in Figure 5 (above), DLBS-LA ($KB = 8, T' = 6$) achieves comparable or even outperforming results with DLBS ($KB = 32$). It is quite beneficial to spend a computation to estimate reward accurately.

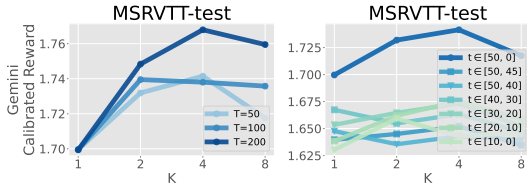


Figure 8. (Left) Scaling the denoising steps T . DLBS benefits from larger T more than BoN ($K = 1$) or GS ($B = 1$). (Right) Range of denoising steps $t \in [50, 0]$ to apply search methods. While Kim et al. (2024) apply GS in the first 5–10 steps, DLBS over the entire diffusion steps yields the largest improvement.

5.3. Scaling Denoising Steps

The last axis is denoising steps; in general, the more denoising steps are, the finer the video generated is (Ho et al., 2020). We investigate (1) whether this also holds in DLBS, (2) how the improvement is compared to other axes, and (3) when we should run DLBS, while Kim et al. (2024) only apply GS in the first 5–10 steps.

Figure 8 (left) shows the performance when increasing the number of denoising steps T . Since DDIM exhibits fast convergence (Song et al., 2021a), BoN with larger T does not improve the reward much. DLBS improves the performance when scaling denoising steps to $T = 200$ more than BoN or GS, which implies that DLBS benefits from larger computation as well as the other axes. As shown in Figure 5 (MSRVTT-test), the reward is comparable to the one in $KB = 16$, although the range of improvement by denoising steps is smaller than the one from the LA estimator. The last point is how many times we should iterate DLBS. As opposed to Kim et al. (2024), Figure 8 (right) shows that applying DLBS for all the steps is much better than that for limited steps. Scaling the timing when we employ DLBS realizes better alignment on a calibrated reward, and the number of time steps may also improve the performance, while the LA estimator is a priority.

5.4. Evaluation with AI Feedback

As discussed in Section 4, we obtain a manageable reward function through the reward calibration, which reduces the cost for frequent evaluation queries in inference-time search. While DLBS efficiently improves the calibrated reward, (Figure 5), a natural question is whether DLBS can also improve the original VLM feedback by optimizing their calibrated rewards. We use each calibrated reward (Figure 4) for DLBS and evaluate the quality with Gemini or GPT-4o. Figure 9 demonstrates that DLBS maximizing calibrated rewards can improve the original preference feedback from VLMs, as we grow the search budget. This highlights that our recipe to design inference-time search, combining reward calibration and beam search, can contribute to improving video quality in general.

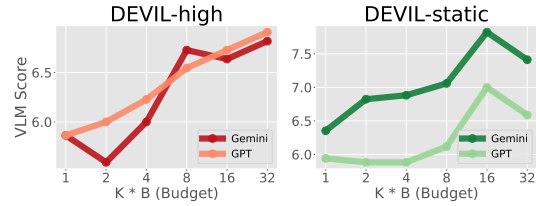


Figure 9. VLM evaluation of video generated with DLBS. As in Figure 5, we use each calibrated reward (Figure 4) for DLBS and evaluate the quality with Gemini or GPT-4o. DLBS on calibrated reward can improve the original preference feedback from VLMs.

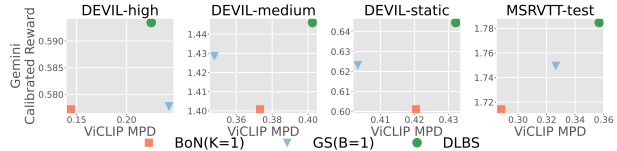


Figure 10. Alignment–diversity tradeoff ($KB = 32$), which is measured by the mean pairwise distance of ViCLIP embeddings. DLBS achieves high performance maintaining higher diversity.

5.5. Alignment–Diversity Tradeoff

Alignment for diffusion models can steer desirable outputs, but it is said that the diversity of generated samples or the performance of original models often degrade (Lee et al., 2023b; Wu et al., 2024b). While inference-time search does not change or degrade the model itself, we here compare the diversity of samples among BoN, GS, and DLBS. We measure the sample diversity as a mean pairwise distance of ViCLIP embeddings (see Appendix J). Figure 10 reveals that DLBS achieves high performance with higher diversity than BoN or GS. This exhibits a benefit from the wider possession and exploration of diffusion latents in DLBS.

6. Related Works

Classifier guidance (Dhariwal & Nichol, 2021; Ho & Salimans, 2022) has been most popular to enhance text-content alignment. On top of that, recent works (Huang et al., 2024a; Li et al., 2024b) leverage reward or external feedback at inference time by selecting better latents (Wallace et al., 2023b), that probably achieve higher reward, during the reverse process. Kim et al. (2025) propose twisted SMC (Wu et al., 2024b) with reward gradient, which is not suitable for non-differentiable feedback and for the domain such as video where reward gradient needs a huge memory cost. Gradient-free methods (Zheng et al., 2024; Ma et al., 2025) such as SMC (Singhal et al., 2025) or greedy search (Kim et al., 2024) often exhibit sub-optimal results affected by inaccurate reward estimate from noisy latents. Yeh et al. (2024) use ODE to estimate the reward, but it highly depends on Karras sampler (Karras et al., 2022) to avoid numerical instability. In contrast, we address the error propagation from inaccurate reward estimate with beam search and lookahead estimator via deterministic DDIM, which is more popular and stable. Our methods work more scalably

when allocating more computation budget at inference time. See [Appendix I](#) for further related works.

7. Discussion and Limitation

We here assume that VLMs work as a proxy of human evaluation, and we demonstrate both qualitative and quantitative improvement of the video quality. It would be important to extend us to scalable methods driven by human feedback not limited to VLMs. While spending more computation at inference time significantly improves perceptual quality, the generation definitely requires more time. It is orthogonal compared to speeding up the sampling process via distillation ([Meng et al., 2022](#); [Song et al., 2023](#)), architecture changes ([Oshima et al., 2024](#)), or parallel sampling ([Shih et al., 2023](#)). We believe both high-quality and speedy sampling have practical needs and should be balanced.

8. Conclusion

This paper studies which metrics we should optimize and how we can optimize them for better text-to-video generation. We point out that feedback from capable VLMs reflects multiple dimensions of video quality so it is insufficient to optimize an existing metric alone, rather we should calibrate the reward by combination. Our DLBS with LA estimator reduces the error propagation from the inaccurate reward estimate. We demonstrate DLBS is the most scalable and robust inference-time search that significantly improves video quality as we increase the search budget, lookahead, and denoising steps. We hope our work encourages more uses of inference-time computation for text-to-video models.

Acknowledgements

We thank Po-Hung Yeh, Shohei Taniguchi, Kuang-Huei Lee, Arnaud Doucet, Heiga Zen, and Yusuke Iwasawa for their support and helpful discussion on the initial idea of this work. HF was supported by JSPS KAKENHI Grant Number JP22J21582, and MS was supported by JSPS KAKENHI Grant Number J23H04974.

Impact Statement

Our work contributes to the progress of text-to-video by focusing on improving the perceptual quality and fidelity of generated videos, specifically addressing issues like unnatural movement, deformation, and temporal inconsistencies, through the inference-time alignment algorithm. Such advancements hold immense potential for revolutionizing creative fields and enabling new applications in gaming, filmmaking, and robotics.

On the other hand, the ability to generate highly realistic

videos raises concerns about the potential for misuse in creating deceptive content, including deepfakes and misinformation. Like other generative models such as large language models, text-to-video models and their inference-time search may inherit and amplify biases present in the training data due to the misalignment. This might lead to the generation of videos that perpetuate harmful stereotypes or underrepresent certain groups.

Lastly, by focusing on inference-time alignment, our method promotes more use of computational resources at test time. On one side, this may increase the environmental footprint for running large generative models and on the other side, our detailed recipe can contribute to designing efficient use of resources and reducing the footprint associated with training. We believe that discussing this aspect is crucial as the scale of these models continues to grow.

References

- Ahn, D., Kang, J., Lee, S., Min, J., Kim, M., Jang, W., Cho, H., Paul, S., Kim, S., Cha, E., Jin, K. H., and Kim, S. A noise is worth diffusion guidance. *arXiv preprint arXiv:2412.03895*, 2024.
- Bai, Y., Kadavath, S., Kundu, S., Aspell, A., Kernion, J., Jones, A., Chen, A., Goldie, A., Mirhoseini, A., McKinnon, C., Chen, C., Olsson, C., Olah, C., Hernandez, D., Drain, D., Ganguli, D., Li, D., Tran-Johnson, E., Perez, E., Kerr, J., Mueller, J., Ladish, J., Landau, J., Ndousse, K., Lukosuite, K., Lovitt, L., Sellitto, M., Elhage, N., Schiefer, N., Mercado, N., DasSarma, N., Lasenby, R., Larson, R., Ringer, S., Johnston, S., Kravec, S., Showk, S. E., Fort, S., Lanham, T., Telleen-Lawton, T., Conerly, T., Henighan, T., Hume, T., Bowman, S. R., Hatfield-Dodds, Z., Mann, B., Amodei, D., Joseph, N., McCandlish, S., Brown, T., and Kaplan, J. Constitutional ai: Harmlessness from ai feedback. *arXiv preprint arXiv:2212.08073*, 2022.
- Bansal, A., Chu, H.-M., Schwarzschild, A., Sengupta, S., Goldblum, M., Geiping, J., and Goldstein, T. Universal guidance for diffusion models. *arXiv preprint arXiv:2302.07121*, 2023.
- Bansal, H., Lin, Z., Xie, T., Zong, Z., Yarom, M., Bitton, Y., Jiang, C., Sun, Y., Chang, K.-W., and Grover, A. Videophy: Evaluating physical commonsense for video generation. *arXiv preprint arXiv:2406.03520*, 2024.
- Black, K., Janner, M., Du, Y., Kostrikov, I., and Levine, S. Training diffusion models with reinforcement learning. In *The Twelfth International Conference on Learning Representations*, 2024.
- Blattmann, A., Dockhorn, T., Kulal, S., Mendeleevitch, D., Kilian, M., Lorenz, D., Levi, Y., English, Z., Voleti, V.,

- Letts, A., Jampani, V., and Rombach, R. Stable video diffusion: Scaling latent video diffusion models to large datasets. *arXiv preprint arXiv:2311.15127*, 2023a.
- Blattmann, A., Rombach, R., Ling, H., Dockhorn, T., Kim, S. W., Fidler, S., and Kreis, K. Align your latents: High-resolution video synthesis with latent diffusion models. In *IEEE Conference on Computer Vision and Pattern Recognition (CVPR)*, 2023b.
- Brooks, T., Peebles, B., Holmes, C., DePue, W., Guo, Y., Jing, L., Schnurr, D., Taylor, J., Luhman, T., Luhman, E., Ng, C., Wang, R., and Ramesh, A. Video generation models as world simulators, 2024. URL <https://openai.com/research/video-generation-models-as-world-simulators>
- Bruce, J., Dennis, M., Edwards, A., Parker-Holder, J., Shi, Y., Hughes, E., Lai, M., Mavalankar, A., Steigerwald, R., Apps, C., et al. Genie: Generative interactive environments. *arXiv preprint arXiv:2402.15391*, 2024.
- Caron, M., Touvron, H., Misra, I., Jégou, H., Mairal, J., Bojanowski, P., and Joulin, A. Emerging properties in self-supervised vision transformers. *arXiv preprint arXiv:2104.14294*, 2021.
- Çiçek, O., Abdulkadir, A., Lienkamp, S. S., Brox, T., and Ronneberger, O. 3d u-net: Learning dense volumetric segmentation from sparse annotation. *arXiv preprint arXiv:1606.06650*, 2016.
- Chen, H., Zhang, Y., Cun, X., Xia, M., Wang, X., Weng, C., and Shan, Y. Videocrafter2: Overcoming data limitations for high-quality video diffusion models. *arXiv preprint arXiv:2401.09047*, 2024.
- Chung, H., Kim, J., Mccann, M. T., Klasky, M. L., and Ye, J. C. Diffusion posterior sampling for general noisy inverse problems. In *The Eleventh International Conference on Learning Representations*, 2023.
- Clark, K., Vicol, P., Swersky, K., and Fleet, D. J. Directly fine-tuning diffusion models on differentiable rewards. In *The Twelfth International Conference on Learning Representations*, 2024.
- Dhariwal, P. and Nichol, A. Q. Diffusion models beat GANs on image synthesis. In *Advances in Neural Information Processing Systems*, 2021.
- Domingo-Enrich, C., Drozdal, M., Karrer, B., and Chen, R. T. Q. Adjoint matching: Fine-tuning flow and diffusion generative models with memoryless stochastic optimal control. *arXiv preprint arXiv:2409.08861*, 2024.
- Dong, H., Xiong, W., Goyal, D., Zhang, Y., Chow, W., Pan, R., Diao, S., Zhang, J., SHUM, K., and Zhang, T. RAFT: Reward ranked finetuning for generative foundation model alignment. *Transactions on Machine Learning Research*, 2023. ISSN 2835-8856.
- Dosovitskiy, A., Beyer, L., Kolesnikov, A., Weissenborn, D., Zhai, X., Unterthiner, T., Dehghani, M., Minderer, M., Heigold, G., Gelly, S., et al. An image is worth 16x16 words: Transformers for image recognition at scale. *arXiv preprint arXiv:2010.11929*, 2020.
- Evans, L. C. Partial differential equations. *American Mathematical Society*, 19, 2022.
- Fan, Y., Watkins, O., Du, Y., Liu, H., Ryu, M., Boutilier, C., Abbeel, P., Ghavamzadeh, M., Lee, K., and Lee, K. Reinforcement learning for fine-tuning text-to-image diffusion models. In *Thirty-seventh Conference on Neural Information Processing Systems*, 2023.
- Fang, Y., Zhu, H., Zeng, Y., Ma, K., and Wang, Z. Perceptual quality assessment of smartphone photography. *Proceedings of the IEEE/CVF Conference on Computer Vision and Pattern Recognition (CVPR)*, 2020.
- Furuta, H., Lee, K.-H., Gu, S. S., Matsuo, Y., Faust, A., Zen, H., and Gur, I. Geometric-averaged preference optimization for soft preference labels. *arXiv preprint arXiv:2409.06691*, 2024a.
- Furuta, H., Zen, H., Schuurmans, D., Faust, A., Matsuo, Y., Liang, P., and Yang, S. Improving dynamic object interactions in text-to-video generation with ai feedback. *arXiv preprint arXiv:2412.02617*, 2024b.
- Gemini Team. Gemini: A family of highly capable multi-modal models. *arXiv preprint arXiv:2312.11805*, 2023.
- Google DeepMind. Veo 2, 2024. URL <https://deepmind.google/technologies/veo/veo-2/>.
- He, X., Jiang, D., Zhang, G., Ku, M., Soni, A., Siu, S., Chen, H., Chandra, A., Jiang, Z., Arulraj, A., Wang, K., Do, Q. D., Ni, Y., Lyu, B., Narsupalli, Y., Fan, R., Lyu, Z., Lin, Y., and Chen, W. Videoscore: Building automatic metrics to simulate fine-grained human feedback for video generation. *arXiv preprint arXiv:2406.15252*, 2024.
- He, Y., Yang, T., Zhang, Y., Shan, Y., and Chen, Q. Latent video diffusion models for high-fidelity long video generation. *arXiv preprint arXiv:2211.13221*, 2022.
- Ho, J. and Salimans, T. Classifier-free diffusion guidance. *arXiv preprint arXiv:2207.12598*, 2022.
- Ho, J., Jain, A., and Abbeel, P. Denoising diffusion probabilistic models. In *Advances in Neural Information Processing Systems*, volume 33, pp. 6840–6851, 2020.

- Hu, E. J., Shen, Y., Wallis, P., Allen-Zhu, Z., Li, Y., Wang, S., Wang, L., and Chen, W. Lora: Low-rank adaptation of large language models. *arXiv preprint arXiv:2106.09685*, 2021.
- Huang, Y., Ghatore, A., Liu, Y., Hu, Z., Zhang, Q., Sastry, C. S., Gururani, S., Oore, S., and Yue, Y. Symbolic music generation with non-differentiable rule guided diffusion, 2024a.
- Huang, Z., He, Y., Yu, J., Zhang, F., Si, C., Jiang, Y., Zhang, Y., Wu, T., Jin, Q., Chanpaisit, N., Wang, Y., Chen, X., Wang, L., Lin, D., Qiao, Y., and Liu, Z. VBench: Comprehensive benchmark suite for video generative models. In *Proceedings of the IEEE/CVF Conference on Computer Vision and Pattern Recognition*, 2024b.
- Karras, T., Aittala, M., Aila, T., and Laine, S. Elucidating the design space of diffusion-based generative models. *arXiv preprint arXiv:2206.00364*, 2022.
- Ke, J., Wang, Q., Wang, Y., Milanfar, P., and Yang, F. Musiq: Multi-scale image quality transformer. *arXiv preprint arXiv:2108.05997*, 2021.
- Kim, J., Kim, B. S., and Ye, J. C. Free²guide: Gradient-free path integral control for enhancing text-to-video generation with large vision-language models. *arXiv preprint arXiv:2411.17041*, 2024.
- Kim, S., Kim, M., and Park, D. Alignment without over-optimization: Training-free solution for diffusion models. *arXiv preprint arXiv:2501.05803*, 2025.
- Kingma, D. P. and Welling, M. Auto-encoding variational bayes. *arXiv preprint arXiv:1312.6114*, 2013.
- LAION-AI. aesthetic-predictor, 2022. URL <https://github.com/LAION-AI/aesthetic-predictor>.
- Lee, H., Phatale, S., Mansoor, H., Mesnard, T., Ferret, J., Lu, K., Bishop, C., Hall, E., Carbune, V., Rastogi, A., and Prakash, S. Rlaif: Scaling reinforcement learning from human feedback with ai feedback. *arXiv preprint arXiv:2309.00267*, 2023a.
- Lee, K., Liu, H., Ryu, M., Watkins, O., Du, Y., Boutilier, C., Abbeel, P., Ghavamzadeh, M., and Gu, S. S. Aligning text-to-image models using human feedback. *arXiv preprint arXiv:2302.12192*, 2023b.
- Li, J., Feng, W., Fu, T.-J., Wang, X., Basu, S., Chen, W., and Wang, W. Y. T2v-turbo: Breaking the quality bottleneck of video consistency model with mixed reward feedback. *arXiv preprint arXiv:2405.18750*, 2024a.
- Li, X., Zhao, Y., Wang, C., Scalia, G., Eraslan, G., Nair, S., Biancalani, T., Ji, S., Regev, A., Levine, S., and Uehara, M. Derivative-free guidance in continuous and discrete diffusion models with soft value-based decoding. *arXiv preprint arXiv:2408.08252*, 2024b.
- Li, Z., Zhu, Z.-L., Han, L.-H., Hou, Q., Guo, C.-L., and Cheng, M.-M. Amt: All-pairs multi-field transforms for efficient frame interpolation. In *Proceedings of the IEEE/CVF Conference on Computer Vision and Pattern Recognition (CVPR)*, 2023.
- Liang, Z., Yuan, Y., Gu, S., Chen, B., Hang, T., Li, J., and Zheng, L. Step-aware preference optimization: Aligning preference with denoising performance at each step. *arXiv preprint arXiv:2406.04314*, 2024.
- Liao, M., Lu, H., Zhang, X., Wan, F., Wang, T., Zhao, Y., Zuo, W., Ye, Q., and Wang, J. Evaluation of text-to-video generation models: A dynamics perspective. *arXiv preprint arXiv:2407.01094*, 2024.
- Liu, S., Ren, Z., Gupta, S., and Wang, S. Physgen: Rigid-body physics-grounded image-to-video generation. In *European Conference on Computer Vision (ECCV)*, 2024.
- Ma, N., Tong, S., Jia, H., Hu, H., Su, Y.-C., Zhang, M., Yang, X., Li, Y., Jaakkola, T., Jia, X., and Xie, S. Inference-time scaling for diffusion models beyond scaling denoising steps. *arXiv preprint arXiv:2501.09732*, 2025.
- Ma, X., Wang, Y., Jia, G., Chen, X., Liu, Z., Li, Y.-F., Chen, C., and Qiao, Y. Latte: Latent diffusion transformer for video generation. *arXiv preprint arXiv:2401.03048*, 2024.
- Ma, Y., Xu, G., Sun, X., Yan, M., Zhang, J., and Ji, R. X-clip: End-to-end multi-grained contrastive learning for video-text retrieval. *arXiv preprint arXiv:2207.07285*, 2022.
- Meng, C., Rombach, R., Gao, R., Kingma, D. P., Ermon, S., Ho, J., and Salimans, T. On distillation of guided diffusion models. *arXiv preprint arXiv:2210.03142*, 2022.
- Moral, P. Feynman-kac formulae: genealogical and interacting particle systems with applications. *Springer*, 2004.
- Na, S., Kim, Y., and Lee, H. Boost your own human image generation model via direct preference optimization with ai feedback. *arXiv preprint arXiv:2405.20216*, 2024.
- OpenAI. Gpt-4 technical report. *arXiv preprint arXiv:2303.08774*, 2023.
- OpenAI. Sora, 2024. URL <https://openai.com/index/sora/>.

- Oshima, Y., Taniguchi, S., Suzuki, M., and Matsuo, Y. Ssm meets video diffusion models: Efficient long-term video generation with structured state spaces. *arXiv preprint arXiv:2403.07711*, 2024.
- Pavon, M. Stochastic control and nonequilibrium thermodynamical systems. *Applied Mathematics and Optimization*, 19:187–202, 1989.
- Prabhudesai, M., Mendonca, R., Qin, Z., Fragkiadaki, K., and Pathak, D. Video diffusion alignment via reward gradients. *arXiv preprint arXiv:2407.08737*, 2024.
- Qi, Z., Bai, L., Xiong, H., and Xie, Z. Not all noises are created equally: diffusion noise selection and optimization. *arXiv preprint arXiv:2407.14041*, 2024.
- Radford, A., Kim, J. W., Hallacy, C., Ramesh, A., Goh, G., Agarwal, S., Sastry, G., Askell, A., Mishkin, P., Clark, J., Krueger, G., and Sutskever, I. Learning transferable visual models from natural language supervision. *arXiv preprint arXiv:2103.00020*, 2021.
- Raffel, C., Shazeer, N., Roberts, A., Lee, K., Narang, S., Matena, M., Zhou, Y., Li, W., and Liu, P. J. Exploring the limits of transfer learning with a unified text-to-text transformer. *Journal of Machine Learning Research*, 21(140):1–67, 2020. URL <http://jmlr.org/papers/v21/20-074.html>.
- Rombach, R., Blattmann, A., Lorenz, D., Esser, P., and Ommer, B. High-resolution image synthesis with latent diffusion models. *arXiv preprint arXiv:2112.10752*, 2022.
- Salimans, T., Goodfellow, I., Zaremba, W., Cheung, V., Radford, A., and Chen, X. Improved techniques for training gans. *arXiv preprint arXiv:1606.03498*, 2016.
- Shih, A., Belkhale, S., Ermon, S., Sadigh, D., and Anari, N. Parallel sampling of diffusion models. In *Thirty-seventh Conference on Neural Information Processing Systems*, 2023.
- Singhal, R., Horvitz, Z., Teehan, R., Ren, M., Yu, Z., McKeown, K., and Ranganath, R. A general framework for inference-time scaling and steering of diffusion models. *arXiv preprint arXiv:2501.06848*, 2025.
- Sohl-Dickstein, J., Weiss, E., Maheswaranathan, N., and Ganguli, S. Deep unsupervised learning using nonequilibrium thermodynamics. In *Proceedings of the 32nd International Conference on Machine Learning*, volume 37, pp. 2256–2265, 2015.
- Song, J., Meng, C., and Ermon, S. Denoising diffusion implicit models. In *International Conference on Learning Representations*, 2021a.
- Song, Y., Sohl-Dickstein, J., Kingma, D. P., Kumar, A., Ermon, S., and Poole, B. Score-based generative modeling through stochastic differential equations. In *International Conference on Learning Representations*, 2021b.
- Song, Y., Dhariwal, P., Chen, M., and Sutskever, I. Consistency models. *arXiv preprint arXiv:2303.01469*, 2023.
- Teed, Z. and Deng, J. Raft: Recurrent all-pairs field transforms for optical flow. *arXiv preprint arxiv:2003.12039*, 2020.
- Uehara, M., Zhao, Y., Black, K., Hajiramezani, E., Scalia, G., Diamant, N. L., Tseng, A. M., Biancalani, T., and Levine, S. Fine-tuning of continuous-time diffusion models as entropy-regularized control. *arXiv preprint arxiv:2402.15194*, 2024.
- Unterthiner, T., van Steenkiste, S., Kurach, K., Marinier, R., Michalski, M., and Gelly, S. Towards accurate generative models of video: A new metric & challenges. *arXiv preprint arXiv:1812.01717*, 2019.
- Wallace, B., Dang, M., Rafailov, R., Zhou, L., Lou, A., Purushwalkam, S., Ermon, S., Xiong, C., Joty, S., and Naik, N. Diffusion model alignment using direct preference optimization. *arXiv preprint arXiv:2311.12908*, 2023a.
- Wallace, B., Gokul, A., Ermon, S., and Naik, N. End-to-end diffusion latent optimization improves classifier guidance. *arXiv preprint arXiv:2303.13703*, 2023b.
- Wang, Z., Bovik, A., Sheikh, H., and Simoncelli, E. Image quality assessment: from error visibility to structural similarity. *IEEE Transactions on Image Processing*, 13(4):600–612, 2004.
- Wu, J. Z., Fang, G., Wu, H., Wang, X., Ge, Y., Cun, X., Zhang, D. J., Liu, J.-W., Gu, Y., Zhao, R., Lin, W., Hsu, W., Shan, Y., and Shou, M. Z. Towards a better metric for text-to-video generation. *arXiv preprint arXiv:2401.07781*, 2024a.
- Wu, L., Trippe, B. L., Naesseth, C. A., Blei, D. M., and Cunningham, J. P. Practical and asymptotically exact conditional sampling in diffusion models. *arXiv preprint arXiv:2306.17775*, 2024b.
- Wu, X., Huang, S., Wang, G., Xiong, J., and Wei, F. Boosting text-to-video generative model with MLLMs feedback. In *The Thirty-eighth Annual Conference on Neural Information Processing Systems*, 2024c.
- Wu, X., Huang, S., and Wei, F. Multimodal large language model is a human-aligned annotator for text-to-image generation. *arXiv preprint arXiv:2404.15100*, 2024d.

- Xu, H., Ghosh, G., Huang, P.-Y., Okhonko, D., Aghajanyan, A., Metze, F., Zettlemoyer, L., and Feichtenhofer, C. Videoclip: Contrastive pre-training for zero-shot video-text understanding. *arXiv preprint arXiv:2109.14084*, 2021.
- Xu, J., Mei, T., Yao, T., and Rui, Y. Msr-vtt: A large video description dataset for bridging video and language. In *Proceedings of the IEEE conference on computer vision and pattern recognition*, pp. 5288–5296, 2016.
- Yang, K., Tao, J., Lyu, J., Ge, C., Chen, J., Li, Q., Shen, W., Zhu, X., and Li, X. Using human feedback to fine-tune diffusion models without any reward model. *arXiv preprint arXiv:2311.13231*, 2023.
- Yeh, P.-H., Lee, K.-H., and Chen, J.-C. Training-free diffusion model alignment with sampling demons. *arXiv preprint arXiv:2410.05760*, 2024.
- Yuan, H., Chen, Z., Ji, K., and Gu, Q. Self-play fine-tuning of diffusion models for text-to-image generation. *arXiv preprint arXiv:2402.10210*, 2024.
- Zhang, R., Isola, P., Efros, A. A., Shechtman, E., and Wang, O. The unreasonable effectiveness of deep features as a perceptual metric. In *CVPR*, 2018.
- Zhang, Y., Tzeng, E., Du, Y., and Kislyuk, D. Large-scale reinforcement learning for diffusion models. *arXiv preprint arXiv:2401.12244*, 2024a.
- Zhang, Z., Zhang, S., Zhan, Y., Luo, Y., Wen, Y., and Tao, D. Confronting reward overoptimization for diffusion models: A perspective of inductive and primacy biases. In *Forty-first International Conference on Machine Learning*, 2024b.
- Zheng, H., Chu, W., Wang, A., Kovachki, N., Baptista, R., and Yue, Y. Ensemble kalman diffusion guidance: A derivative-free method for inverse problems, 2024.
- Zhou, Z., Shao, S., Bai, L., Xu, Z., Han, B., and Xie, Z. Golden noise for diffusion models: A learning framework. *arXiv preprint arXiv:2411.09502*, 2024.
- Zhu, J., Yang, H., He, H., Wang, W., Tuo, Z., Cheng, W.-H., Gao, L., Song, J., and Fu, J. Moviefactory: Automatic movie creation from text using large generative models for language and images. In *Proceedings of the 31st ACM International Conference on Multimedia*, pp. 9313–9319, 2023.
- Øksendal, B. Stochastic differential equations. *Springer*, 2003.

A. Implementation Details

We use the pre-trained T2V diffusion model Latte (Ma et al., 2024), a T5-conditioned (Raffel et al., 2020) Latent Diffusion Transformer-based framework with 1.1B parameters. Our implementation is based on the publicly available code repository at <https://github.com/Vchitect/Latte>, and we utilize the released checkpoint from <https://huggingface.co/maxin-cn/Latte-1>.

Following the original configuration of Latte, we employ a linear noise schedule with $\beta_{\text{start}} = 0.0001$ and $\beta_{\text{end}} = 0.02$, and set the guidance scale $w_{\text{cfg}} = 7.5$ for all experiments.

All experiments are conducted in half precision (fp16) on a single NVIDIA A100 GPU (40 GB) with a batch size of 1. We report generation times for various configurations of the diffusion steps T , the lookahead steps T' , and the search budget KB . The approximate time consumption for different settings is summarized in Table 1.

For AI feedback, we use API endpoints: gpt-4o-2024-11-20 and gemini-1.5-pro-002.

Table 1. Approximate video generation time (minutes) for different settings of the diffusion steps T , the lookahead steps T' , and the search budget KB on a single NVIDIA A100 GPU (40 GB) with a batch size of 1, using the Gemini Calibrated Reward for MSRVT-test.

T	T'	KB	Execution Time (min)
50	1	4	11
50	1	8	22
50	1	16	45
50	1	32	90
50	6	8	30
100	1	8	45
200	1	8	90

B. Details of Metric Rewards

Subject Consistency We adopt the subject consistency metric proposed in VBench (Huang et al., 2024b) to quantify how consistently a subject is depicted across consecutive video frames. Concretely, for each frame i in a video, we extract a feature representation \mathbf{d}_i using DINO (Caron et al., 2021) with a ViT-B/16 (Dosovitskiy et al., 2020) backbone. Let $\langle \mathbf{d}_i, \mathbf{d}_j \rangle$ denote the cosine similarity between the features \mathbf{d}_i and \mathbf{d}_j . Then, VBench defines the subject consistency metric as follows:

$$R_{\text{subject}} = \frac{1}{T-1} \sum_{t=2}^T \frac{1}{2} (\langle \mathbf{d}_1, \mathbf{d}_t \rangle + \langle \mathbf{d}_{t-1}, \mathbf{d}_t \rangle). \quad (12)$$

DINO, which is trained in a self-supervised manner using unlabeled images and image augmentations, does not explicitly suppress intra-class variations. As a result, it remains particularly sensitive to identity shifts within the same subject, making it well-suited for evaluating subject consistency across frames.

Motion Smoothness We adopt the frame-interpolation-based metric originally proposed in VBench (Huang et al., 2024b) to assess whether a generated video’s motion is smooth and physically plausible. In particular, this metric leverages the motion prior from AMT (Li et al., 2023), employing its AMT-S variant for frame reconstruction. Concretely, let $[\mathbf{f}_0, \mathbf{f}_1, \mathbf{f}_2, \dots, \mathbf{f}_{2n}]$ denote the frames of a generated video. We remove each odd-numbered frame to obtain a lower-frame-rate sequence $[\mathbf{f}_0, \mathbf{f}_2, \mathbf{f}_4, \dots, \mathbf{f}_{2n}]$, and rely on AMT-S to reconstruct the missing frames $[\hat{\mathbf{f}}_1, \hat{\mathbf{f}}_3, \dots, \hat{\mathbf{f}}_{2n-1}]$. We then compute the Mean Absolute Error (MAE) between these reconstructed frames and the original odd-numbered frames, denoting this measure by $R_{\text{smoothness}}$. Finally, following the normalization scheme introduced in VBench, we define:

$$R_{\text{smoothness-norm}} = \frac{255 - R_{\text{smoothness}}}{255}, \quad (13)$$

which ensures that the final score lies in the range $[0, 1]$, with higher values indicating smoother motion. This measure leverages the motion prior in AMT to evaluate whether the generated video’s motion is smooth and physically plausible. We remove each odd-numbered frame, then use AMT-S to reconstruct those frames based on short-term motion assumptions.

Dynamic Degree This measure quantifies the overall magnitude of dynamic object movement. Let T be the total number of frames in the generated video. For each pair of consecutive frames t and $t + 1$, we estimate the optical flow \mathbf{v}_t using RAFT (Teed & Deng, 2020), compute its norm $\|\mathbf{v}_t\|$, and sum these values across all frames:

$$R_{\text{dynamics}} = \sum_{t=1}^{T-1} \|\mathbf{v}_t\|. \quad (14)$$

We then apply a logarithmic transformation to R_{dynamics} and divide by 16:

$$R_{\text{dynamics-rescaled}} = \frac{\log(R_{\text{dynamics}})}{16}. \quad (15)$$

This rescaling helps ensure that the value range of $R_{\text{dynamics-rescaled}}$ is roughly comparable to other metrics in our evaluation.

Aesthetic Quality This criterion evaluates compositional rules, color harmony, and overall artistic merit on a per-frame basis. Concretely, for each frame i in a video, we extract a CLIP image embedding $\mathbf{c}_i^{\text{image}}$ using the CLIP ViT-L/14 model (Radford et al., 2021). We then feed $\mathbf{c}_i^{\text{image}}$ into the LAION aesthetic predictor (LAION-AI, 2022), which assigns a raw rating $r_i \in [0, 10]$. To normalize these scores to the $[0, 1]$ range, we set

$$r'_i = \frac{r_i}{10}. \quad (16)$$

Let T be the total number of frames. The final aesthetic reward is then obtained by taking the average of the normalized ratings across all frames:

$$R_{\text{aesthetic}} = \frac{1}{T} \sum_{i=1}^T r'_i. \quad (17)$$

Because the LAION aesthetic predictor leverages CLIP embeddings instead of raw images, it captures higher-level features related to composition, color harmony, and artistic appeal.

Imaging Quality This indicator assesses low-level distortions (e.g., over-exposure, noise, blur) in each generated frame. We adopt the MUSIQ predictor (Ke et al., 2021), trained on the SPAQ dataset (Fang et al., 2020). The frame-wise score is normalized to $[0, 1]$ by dividing by 100, and the final video score is the mean of these normalized values across all frames in the same way as Equation 16 and Equation 17.

Text-Video Consistency This measure captures how closely a generated video’s content aligns with its text prompt. We employ ViCLIP (Xu et al., 2021), a model pre-trained on a 10M video-text dataset and fine-tuned to handle temporal relationships, to embed both the video frames and the text. Since ViCLIP computes embeddings from 8-frame inputs, we sample 8 frames from 16-frame video. Let $\mathbf{v}^{\text{video}}$ denote the resulting video embedding and \mathbf{v}^{text} denote the text embedding. We then define the final alignment score as the cosine similarity between these embeddings:

$$R_{\text{tv-consistency}} = \langle \mathbf{v}^{\text{video}}, \mathbf{v}^{\text{text}} \rangle \quad (18)$$

C. List of Prompts

MSRVTT-test

1. a woman is singing on stage about that one person being the one she wants
2. someone is filming a parked car in the parking lot
3. a cat is feed it s babies and a rabbit
4. mario game with bombs
5. someone is browsing a set of games on their console
6. a game is being played
7. a man holds a very large stick
8. a yellow-haired girl is explaining about a game
9. a ship is sailing around on the water
10. a woman with blonde hair and a black shirt is talking
11. a buffalo is attacking a man
12. a band is playing music and people are dancing
13. a child is playing a video game
14. a person is showing how to fold paper
15. a woman is sitting down on a couch in a room
16. a man inside of a car is using his finger to point
17. a man waters his plants
18. the symmetrical cone is japan s most famous symbol
19. an indoor soccer game
20. a japanese monkey bathing in a hot spring with pleasant music
21. some images of motorcycles are being shown on tv
22. someone is serving food in the restaurand
23. this is a competition type show
24. a woman on the news is talking about a story
25. this is a phone review video
26. some fake horses are standing around in a game
27. a person is filming a white car interior seat
28. video of clips from a movie
29. a man with a blue and white shirt is walking around
30. person making something in the kitchen

DEVIL-high

1. A bookshelf collapses loudly, books flying everywhere, creating chaos in the once quiet room.
2. Swift scenes of a sandstorm engulfing a desert oasis, with dunes shifting and palm trees bending in the relentless wind.
3. A chaotic scene of cowboys rounding up cattle during a stampede.
4. Suddenly, a storm hits the city, rain pouring down like a torrent, making rivers on the streets.
5. WWI biplanes in a dogfight with canvas wings ripping, dramatic cloud backdrop, ultra-detailed.
6. In the mountains, a bear erupts from the snow, creating a large cloud of powder.
7. Amidst a thunderstorm, a lightning bolt strikes a bicycle, setting it ablaze with crackling energy and lighting up the dark, rainy street.
8. A single eagle dives extremely fast, snatching a fish from the water.
9. A boat hits a big wave and flips, landing upside down.
10. A car drives through a wall of fire in a daring escape.
11. The cat tore across the living room, jumping over toys and furniture to catch the mouse.
12. A cow jumps over a fence, landing in a pond with a big splash.
13. Two dogs chase each other, suddenly skidding around a sharp corner.
14. A storm sweeps an elephant into a raging river, carrying it away swiftly.
15. Racing the sunset, a giraffe charges across the horizon, shadows stretching long.
16. Against the wind, a lone horse gallops, mane streaming behind.
17. Jumping over a gorge, the motorcycle lands just in time on the other side.
18. A thief sprints away from the scene, with the police in hot pursuit.
19. The ice cracks beneath their feet, making the sheep skid and slide, rushing to solid ground.
20. Lightning strikes as a train blasts its horn, cutting through a stormy night.
21. A truck speeds across the desert, dust clouds swirling behind it.
22. Under a rainbow, a zebra kicks up a spray of water as it crosses a fast-flowing river.

DEVIL-medium

1. London heathrow, united kingdom - 05 12 2019: 4k super-telephoto plane accelerates down hot runway through heat shimmer
2. A cool dj teddy bear with sunglasses on top of turntable with video static
3. Aerial view. cute girl in the coat drive on country road on the bicycle
4. Brown pelican flying flight in fall bay harbor in ecuador
5. Small fishing boat, anchored on a silver ocean, in thailand.
6. a filled yellow school bus with over-sized black wheels drives through a flooded area with red lights on and gets splattered with mud
7. St. petersburg, russia - circa march, 2015: vehicles drive on city ringroad at evening time. st. petersburg ring road is a main route encircling the city
8. cat manages to hang on to dangling object
9. Taking cow milk cheese with fork 4k footage
10. dog passes in and out of view
11. 1930s: elephant roars, man shoots at elephant. elephants walk through jungle. man tries to fire gun, throws gun on ground, runs away.
12. the baby giraffe is zoomed in on and then camera shakes
13. Cowboys drive group of horses at farming enterprise.
14. 4k couple watching film or tv at home & jumping with shock at the action
15. contestants are reading themselves to start a mini-motorbike race
16. Macao beach with stone mountains aerial view from drone. travel destination. summer vacation. dominican republic
17. Male boxer resting and sweating after boxing training
18. Wild tulips in a meadow on background sky. sunrise. bonfire. a quiet spring morning in the steppe.
19. Sheep eating grass in punata and potosi, bolivia.
20. Bodo arctic town norway - ca july 2018: train station building and rails tilt up
21. a woman is describing different sets of tubes and hoses in the back of a white pick up truck which is parked on the side of a street with cars going by in the background
22. Istanbul, turkey - october 2018: commuters inside istanbul metro wagon travelling towards taksim station

DEVIL-static

1. airplane with red body is shown for first time.
2. a man holds up a stuffed bear.
3. when you can see the first view of the full bike
4. second bird lands on feedersecond bird lands on feeder
5. a red boat is first seen.
6. Tourist bus station 3d realistic footage. public transport front view animation. vehicles on modern urban highway bridge background. passengers transportation parking. city bus stop video
7. black car is under the blue sign.
8. cat looks at the camera
9. dog puts paws together
10. a white horse standing beside red colored wearing girl dress standing with stick bending down knee displaying on screen
11. Blurred conference room with audience - 4k video
12. first time we see orange branch to the right
13. A woman and a man. holding a gift.
14. A tranquil tableau of the old red barn stood weathered and iconic against the backdrop of the countryside
15. black numbers 1758 at bottomof train
16. a large white box truck travels through water is followed by two other trucks and ascends a gray road through mountains
17. view of big city from balconyview of big city from balcony

D. Detailed Analysis on Reward Function for Perceptual Video Quality

Figure 11 shows that different metrics in reward functions for perceptual video quality often exhibit negative or weak correlations. For example, dynamic degree tends to be negatively correlated with many other metrics, indicating that optimizing exclusively for one metric can either reduce motion dynamics or undermine temporal consistency and aesthetic quality. These findings underscore the need to balance potentially conflicting reward functions rather than prioritizing any single one in isolation, emphasizing the importance of a carefully calibrated approach to evaluating generated videos.

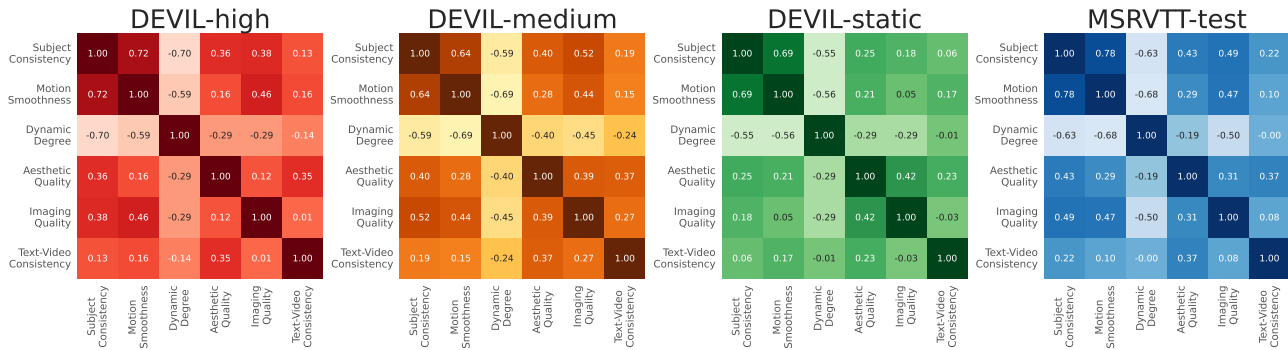


Figure 11. Correlation between reward functions for perceptual video quality.

E. Prompt for AI Feedback

Prompt for AI Feedback from VLMs

You are a helpful assistant that evaluates the quality of a generated video from a textual prompt.

Compare the text prompt and generated video and evaluate the quality (visual quality, proper dynamics, etc...) of the video.

First explain the reasoning, then present the final assessment. Start the reasoning with 'Reasoning: '.

After explaining the reasoning, present the final assessment with 'Assessment: '.

Your final 'Assessment' should be a single-number score from 1 to 10, not as a fraction.

When evaluating, consider the following points:

- Visual Quality: Evaluate the clearness, resolution, brightness, aesthetic appeal of the video.
- Dynamics: Evaluate whether the video demonstrates appropriate dynamics, ensuring it avoids excessive movement in situations meant to be static or insufficient movement in situations intended to be dynamic.
- Smoothness, Consistency, and Naturalness: Assess the smoothness, consistency, and naturalness of shape and motion for objects, animals, and humans.
- Contents: Evaluate whether the video content aligns with the given text prompt.

Textual Prompt: {instruction}

Video: {video_file}

F. Calibrating Reward to Preference Feedback from GPT-4o

Figure 12 shows the two dimensional histogram and correlation between reward function and AI feedback from GPT-4o (OpenAI, 2023), and Figure 13 represent the coefficient of calibrated reward designed for GPT-4.

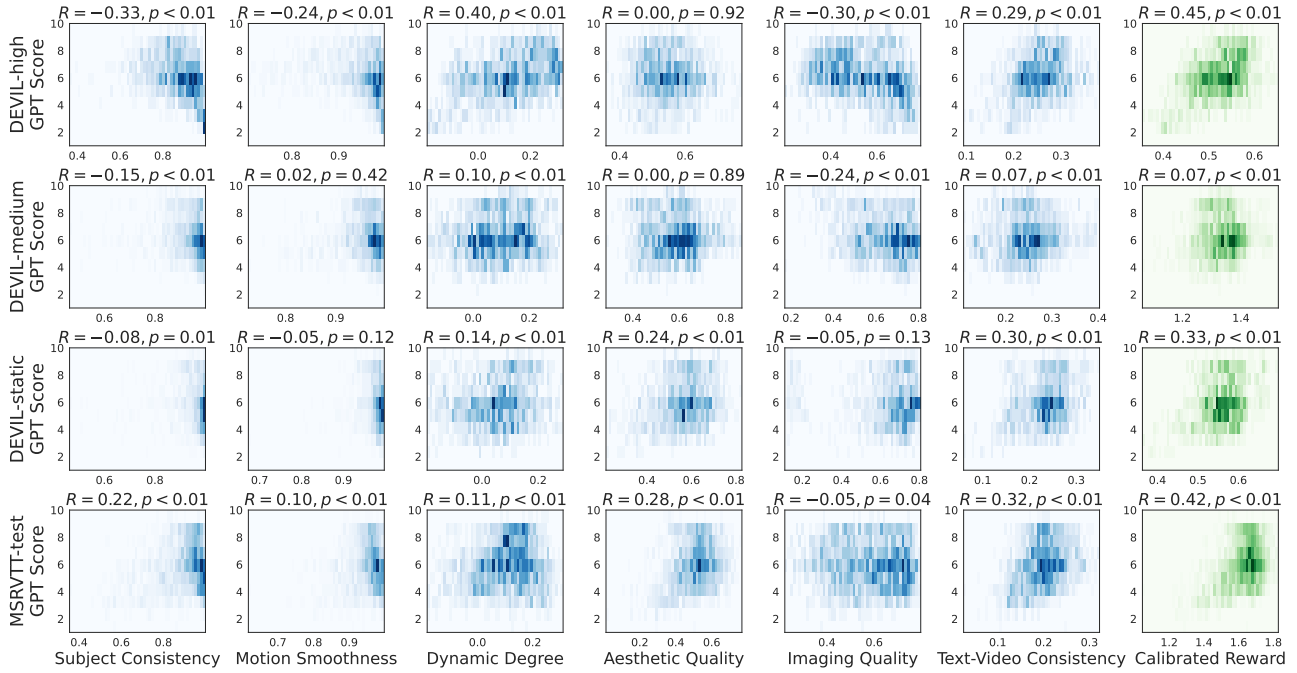


Figure 12. 2D-histogram and correlation between reward function and AI feedback from GPT-4o.

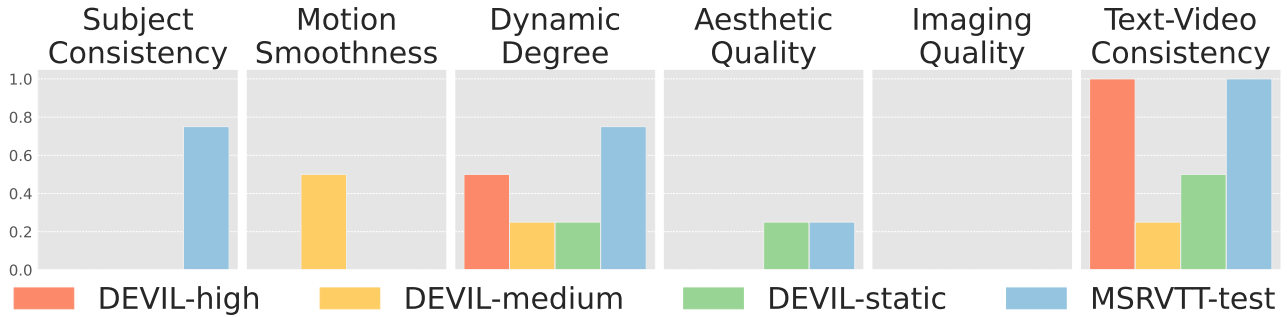


Figure 13. Coefficients of calibrated reward with GPT-4o.

G. Qualitative Evaluation

We provide example videos among individual rewards and VLM calibrated rewards in Figure 14.



Figure 14. We selected the video with the highest reward from 64 randomly generated videos. Videos chosen based on subject consistency or motion smoothness tend to lack motion, while those selected based on dynamic degree or imaging quality often fail to adhere to the given prompt. Additionally, evaluations based on dynamic degree may also lead to a loss of temporal consistency. Text-video consistency often exhibits a high correlation with VLM-based evaluation and, among individual metrics (Figure 3), is relatively effective in capturing the overall quality of a video. However, it may overlook certain aspects, such as frame-wise artifacts. Videos selected by VLM-calibrated rewards demonstrate a more balanced quality.

H. Additional Results for Inference-Time Text-to-Video Alignment

Figure 15 illustrates how varying the value of η in DDIM influences search performance. Here, η controls the degree of randomness in the DDIM scheduler: $\eta = 0.0$ corresponds to the deterministic version of DDIM, while $\eta = 1.0$ is equivalent to DDPM. As η decreases below 1.0, performance in terms of the final reward diminishes, presumably because lowering the randomness in the sampling process narrows the scope of exploration.

Figure 16 the performance of inference-time search on DEVIL-medium that includes the results with $KB = 64$. We can observe that the increasing trends still continue.

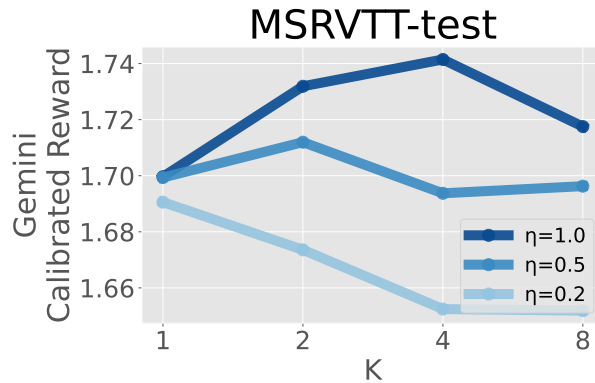


Figure 15. Comparison among different η in DDIM sampler.

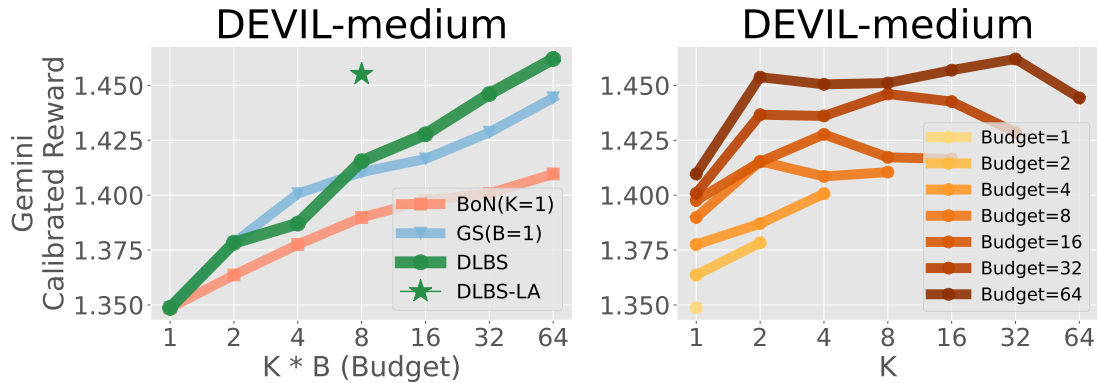


Figure 16. Inference-time search on reward calibrated to Gemini including $KB = 64$.

I. Extended Related Works

Aligning Diffusion Models via Finetuning Alignment by finetuning text-conditioned models has been investigated for image (Lee et al., 2023b) and video (Furuta et al., 2024b; Wu et al., 2024c) generation. Typically, LoRA (Hu et al., 2021) in a backbone model (Çiçek et al., 2016) is finetuned through policy gradient (Black et al., 2024; Fan et al., 2023; Zhang et al., 2024a), direct preference optimization (Yuan et al., 2024; Na et al., 2024; Yang et al., 2023; Liang et al., 2024; Wallace et al., 2023a), reward-weighted regression (Dong et al., 2023), or direct reward gradient (Prabhudesai et al., 2024; Clark et al., 2024; Wu et al., 2024c; Li et al., 2024a). Some train an extra model for better initial noise space (Qi et al., 2024; Ahn et al., 2024; Zhou et al., 2024). In contrast, we focus on the search over the denoising process at inference time, which does not require any model updates and may not degrade the original performance.

Evaluation of Text-to-Video Generation While there are several conventional metrics for video generation (or the one repurposed from image generation) such as SSIM (Wang et al., 2004), IS (Salimans et al., 2016), LPIPS (Zhang et al., 2018), or FVD (Unterthiner et al., 2019), those are not always suitable to evaluate how the quality of contents in video is, which is much more emphasized in text-to-video generation (Wu et al., 2024a). It has been a long-standing challenge to comprehensively and semantically evaluate the dynamics of contents or physical commonsense in generated videos (Bansal et al., 2024; Liao et al., 2024). To deal with that, VBench (Huang et al., 2024b) is recently proposed as a suite of holistic evaluations for text-to-video generation to reflect the perceptual aspect of the quality, such as consistency, smoothness, aesthetics of contents or text–video alignment. Moreover, inspired by the success in LLMs (Bai et al., 2022; Lee et al., 2023a; Furuta et al., 2024a), we could leverage VLMs, which become more capable these days, as a proxy of human evaluation of the contents (Wu et al., 2024c); by finetuning CLIP-based models (He et al., 2024; Radford et al., 2021; Ma et al., 2022), or prompting GPT-4o (OpenAI, 2023) or Gemini (Gemini Team, 2023). Our paper adopts AI feedback from VLMs as an alternative to human rater, and proposes a recipe to calibrate a reward to other sources of feedback (such as AI or human feedback), by considering a linear combination of fine-grained metrics.

J. Details of Sample Diversity

We compute the pairwise distances of ViCLIP (Xu et al., 2021) embeddings for video generation to quantify the diversity in videos, inspired by the approach for evaluating diversity in images (Kim et al., 2025). Specifically, given N generated video samples, we first extract ViCLIP embeddings $\mathbf{v}^{\text{video},(i)}$ for each sample i . The pairwise diversity score is then computed as the mean pairwise distance:

$$D_{\text{video-diversity}} = \frac{1}{N(N-1)} \sum_{i \neq j} \left(1 - \langle \mathbf{v}^{\text{video},(i)}, \mathbf{v}^{\text{video},(j)} \rangle \right). \tag{19}$$

Here, $\langle \mathbf{v}^{\text{video},(i)}, \mathbf{v}^{\text{video},(j)} \rangle$ denotes the cosine similarity between the ViCLIP embeddings of two generated videos i and j . This formulation is similar to Equation 18, but in the case of pairwise distance computation, we take the pairwise mean of $1 - (\text{cosine similarity})$ to obtain a diversity measure.